Soil Dynamics and Earthquake Engineering xxx (xxxx) xxx–xxx

Contents lists available at ScienceDirect

Soil Dynamics and Earthquake Engineering

journal homepage: www.elsevier.com/locate/soildyn

Emulative seismic resistant technology for Accelerated Bridge Construction

Mustafa Mashal[a,*], Alessandro Palermo[b]

[a] Idaho State University, 921 S 8th Avenue, MS 8060, Pocatello, ID 83209, United States
[b] University of Canterbury, 69 Creyke Road, Christchurch 8041, New Zealand

ARTICLE INFO

Keywords:
Accelerated Bridge Construction
Emulative connections
Seismic design
Prefabrication
Experimental testing
Bridges
Member socket connection
Grouted ducts connection

ABSTRACT

Accelerated Bridge Construction (ABC) offers advantages such as rapid construction, limited traffic disruption, fast project delivery, cost savings for the formwork, more accuracy in construction due to prefabrication, better quality control, higher durability, reduced weight of the bridge structure, enhanced safety, and less environmental impacts. ABC has been successfully deployed in low seismic regions. However, given the uncertainty about the adequate performance of connections between precast elements, application of ABC in high seismic regions has been limited. The research investigates the use of two types of emulative connections in a precast bent. The column-to-footing connection consists of member socket, while the column-to-cap beam connection is grouted ducts. These connections intend to emulate the traditional formation of plastic hinges in the bridge columns during an earthquake. A half-scale specimens with emulative connections was tested under quasi-static cyclic loading. Experimental results showed adequate seismic performance of the specimen compared to cast-in-place construction.

1. Introduction

Accelerated Bridge Construction (ABC) has been gaining popularity among many Departments of Transportation (DOTs) in the United States, and other countries. Past studies on ABC include Billington et al. [1,2], Wacker et al. [3], Restrepo et al. [4], Marsh et al. [5], Mashal and Palermo [6], Sideris et al. [7], Mashal et al. [8], Haber [9], Khaleghi [10], and others. There have been many applications of ABC in low seismic regions. However, observations from the past earthquakes have raised concerns about seismic performance of the connections between precast elements (Buckle [11] and Hawkins et al. [12]).

Emulative cast-in-place connections for bridge structures aim to achieve the common plastic hinging of the columns that occurs in cast-in-place construction. Over the years, a variety of these connections have been developed which includes bar couplers, grouted ducts, pocket, and member socket connections. From these emulative connections, the grouted ducts and member socket connections have been selected in this research. While these connections have been previously investigated in cantilever columns by Mashal et al. [8] and others, they had not been tested together in a precast bent system. Marsh et al. [5] presents a concept for a precast bent in seismic regions (Fig. 1). In this concept, column-to-footing connection is member socket, while column-to-cap beam connection is grouted ducts. A brief description of grouted ducts and member socket connections, are presented in the following sections.

In Fig. 1, the column can be either segmental or in one piece. Plastic hinges are expected to be formed at the top and bottom of the bridge columns during a design level earthquake. The footings and cap beam are capacity protected elements. This means that there should not be any inelastic action occurring in these elements during the earthquake. The columns are the sacrificial elements in this instance. Column-to-footing and column-to-cap beam connections would need to be strong enough to push the damage (plastic hinging) away from the panel zones into the columns. For a bent comprised of two columns, there would be four plastic hinges forming at the top and bottom of the columns during an earthquake.

1.1. Grouted ducts connection

Grouted ducts connection is an emulative cast-in-place connection in which the starter bars from one member are extended into the ducts placed during the prefabrication inside the second member (Fig. 2). The ducts are later fully grouted using high-strength grout to secure the connection. Once the grout is hardened, it confines the bars inside the ducts. Mashal et al. [8] investigated the concept of leaving an unbonded (taped) length in the starter bars in a grout ducts connection. Experimental results showed enhanced ductility and energy dissipation of the connection with the unbonded length of the starter bars.

* Corresponding author.
E-mail addresses: mashmust@isu.edu (M. Mashal), alessandro.palermo@canterbury.ac.nz (A. Palermo).

https://doi.org/10.1016/j.soildyn.2018.12.016
Received 30 April 2018; Received in revised form 20 October 2018; Accepted 16 December 2018

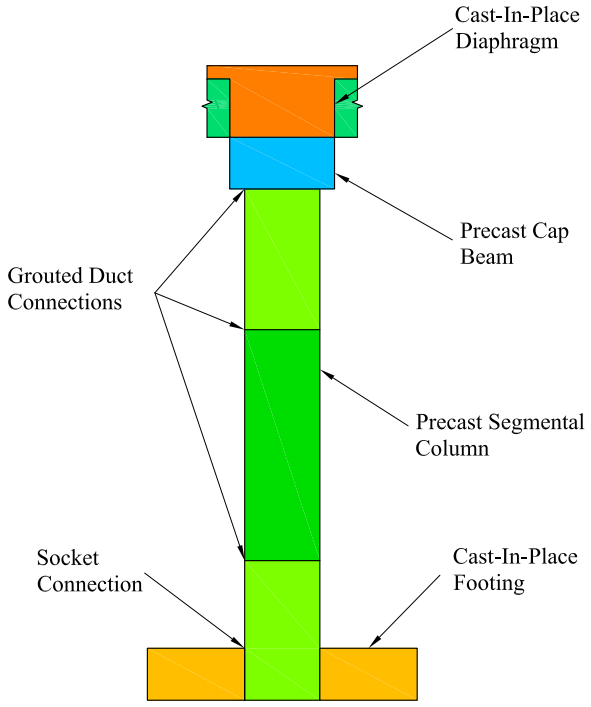

Fig. 1. Concept for a precast bent in seismic regions [5].

Grouted ducts connection can be used for pile-to-pile cap, column-to-cap beam, and for splices between the column or cap beam segments. Grouted ducts connection has already been used in non-seismic and seismic regions. There is a significant amount of research done on grouted ducts connection. Past research include Matsumoto et al. [13,14], Brenes et al. [15], Riva [16], Culmo [17], Steuck and Stanton [18], Pang et al. [19], Haraldsson et al. [20], Restrepo et al. [4], and Mashal et al. [8].

1.2. Member socket connection

Member socket is another type of emulative cast-in-place connection which is formed by embedding a precast element inside another element. The second element can be either precast or cast-in-place. If both elements are precast, the connection is secured using a high-strength grout, or concrete closure-pour in the preformed socket (Fig. 3). The other solution is to have the second element cast around the first one, as shown in Fig. 3. In a member socket connection, there is no crossing of reinforcing bars at the column to footing interface. There is also no steel tube confining the concrete column. The end region of the columns and socket walls in the footing can be left with exposed aggregates for a better bond.

Member socket connection can be used for footing-to-column, column-to-cap beam, and pile-to-pile cap connections. The connection was previously investigated and experimentally tested by Haraldsson et al. [20] and Mashal et al. [8]. More details on the socket connection can be found in Riva [16]. A variation of member socket connection is Concrete-Filled Steel Tubes (CFST). Past research on CFST include Marson and Bruneau [21], Kingsley [22], Zhu et al. [23], Nelson et al. [24], Roeder et al. [25], and Culmo [17].

2. Prototype structure

The prototype structure consists of a multi-column pier system (bent) for a typical highway bridge in New Zealand (Fig. 4). The bridge has six spans. Each span is 16 m which gives a total length of 96 m for the bridge. The height from top of the footing up to the center of mass of the bridge is taken to be 5.8 m. The overall width of the bridge is taken to be 10.4 m. The superstructure is consisted of I-beam 1600 deck system in accordance with NZTA 364 Report [26]. The prototype bridge is assumed to be located on non-liquefiable soils. Base supports are assumed to be fully fixed with no soil-structure interaction. It is important to note that the footing system shown in Fig. 4 for the prototype structure is only indicative.

3. Development of the specimen

Using the prototype structure in Fig. 4, a half-scale specimen was developed based on the concept presented by Marsh et al. [5] for a precast bent in seismic regions. The half-scale specimen is shown in Fig. 5.

Seismic design parameters for the bent were adopted in accordance with New Zealand Bridge Manual 3rd Edition [27] and New Zealand Standards 1170.5 [28]. Table 1 presents a summary of the seismic parameters for the half-scale bent.

4. Design considerations and construction of the specimen

The half-scale bent was designed in accordance with NZS 3101 [29]. Concrete compressive strength at 28-day for the columns, cap beam, and footings was close to 50 MPa. A similar value was obtained from testing of grout samples as well. All reinforcing bars were grade 500 MPa.

Detailed design considerations for the grouted ducts connections can be found in [8]. A summary is presented here. For the column-to-cap beam grouted ducts connection in the bent, an internal shear key was incorporated at the interface level. The top of the column had a

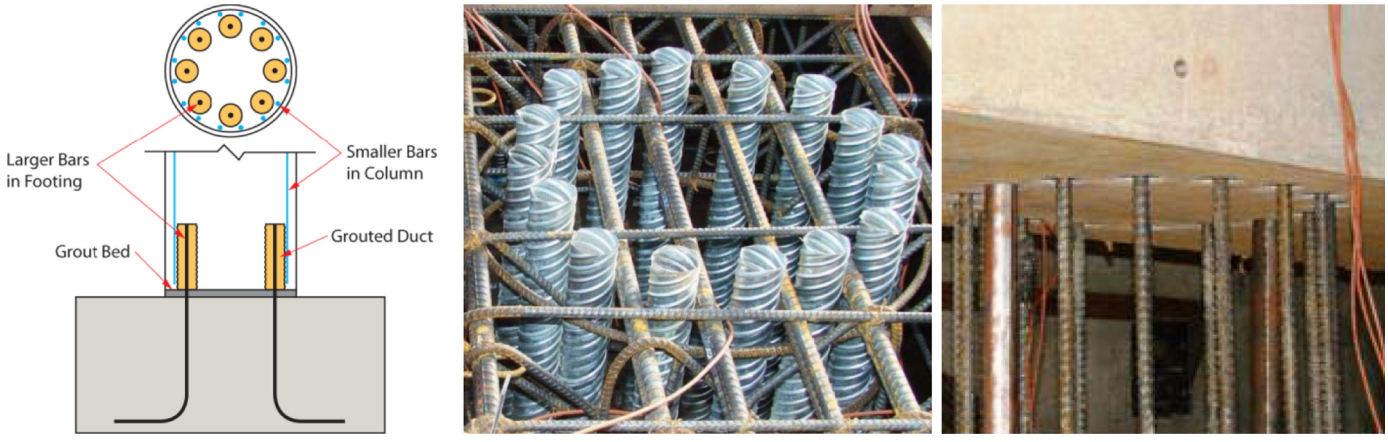

Fig. 2. Arrangements in a Grouted Ducts Connection.

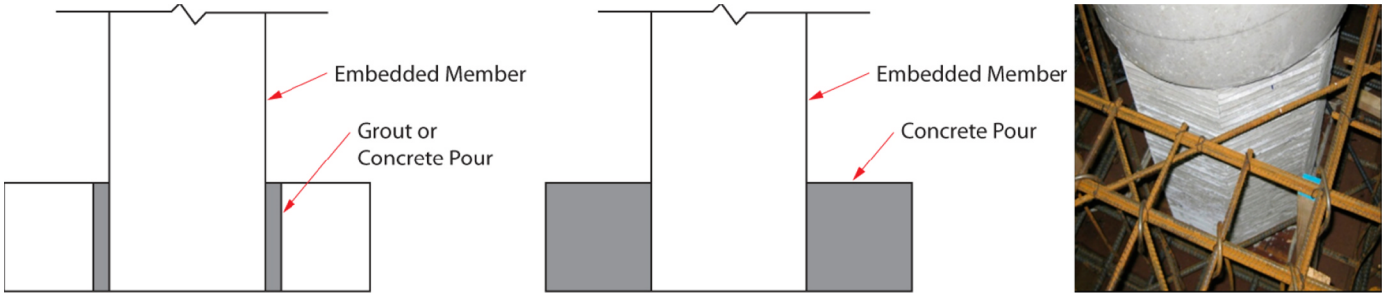

Fig. 3. Arrangements in a member socket connection.

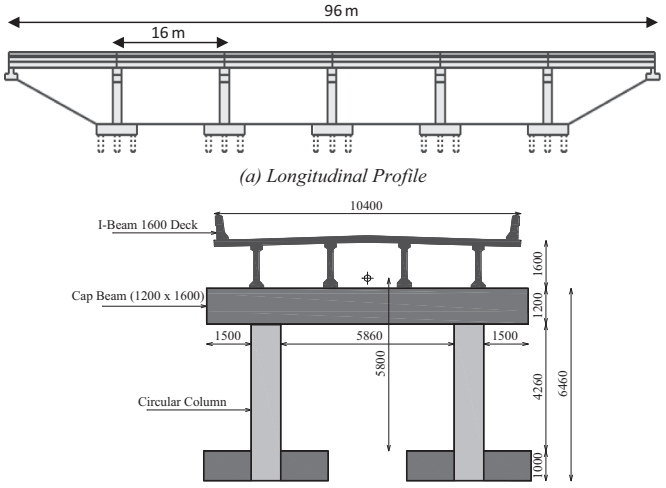

Fig. 4. Details of prototype bridge (all dimensions are in mm).

recess (Fig. 6c) to accommodate the shear key from the cap beam (Fig. 7a). The shear key was intended to provide more ductility for the bent, and would let the starter bars to work in flexural action only. Grouted ducts provide enhanced confinement for the starter bars which can cause issues such as strain concentrations at the interface level. In order to improve the fatigue performance of the starter bars under cyclic loading, there was a 100 mm unbonded (taped) length of the starter bars just under the interface in the column (Fig. 6b).

General design considerations for the member socket connection includes the depth of the socket, column diameter, relative size of the socket to column diameter, roughened surface for the column stub and socket walls, and foot inserts for the column reinforcing bars. The socket depth needs to be sufficient to safely transfer lateral and gravity loads from the column to the footing. In this research a ratio of 1:1 was used for the socket depth to column diameter. Previous work by [8,30] showed that keeping such a ratio would concentrate the damage to the column, not the footing socket. The socket wall in the footing and the concrete surface of the column stub were roughened with exposed aggregates during the prefabrication process. This technique provides a better bond for the connection. The exposed aggregates surface was left in saturated surface dry condition before pouring the grout. Foot inserts were provided at the end of the column rebars to provide safety against any rebar pull-out effects during cyclic loading. Further detailed design considerations for member socket connection can be found in [8] and [20].

Table 1
Summary of the seismic design parameters.

Seismic Hazard Factor, Z	0.29
Soil Class	E (Soft Soils)
Return Period, T_R	2500 Years
Return Period Factor, R	1.8
Near Fault Factor, N	1
Assumed Ductility, μ (ULS)	3
Structural performance Factor, S_p	0.7
Fundamental Natural Period, T (NZS 1170.5)	0.24 s
Fundamental Natural Period, T (Modal Analysis)	0.23 s
Self-weight of Bent, W_{sw}	80 kN
Superstructure weight, W_{sp}	390 kN
Design Gravity Load, W (W_{sw} + W_{sp})	470 kN
Design Lateral Load, V	305 kN
Seismic Coefficient (V/W)	0.65
Design Drift (%)	2.2

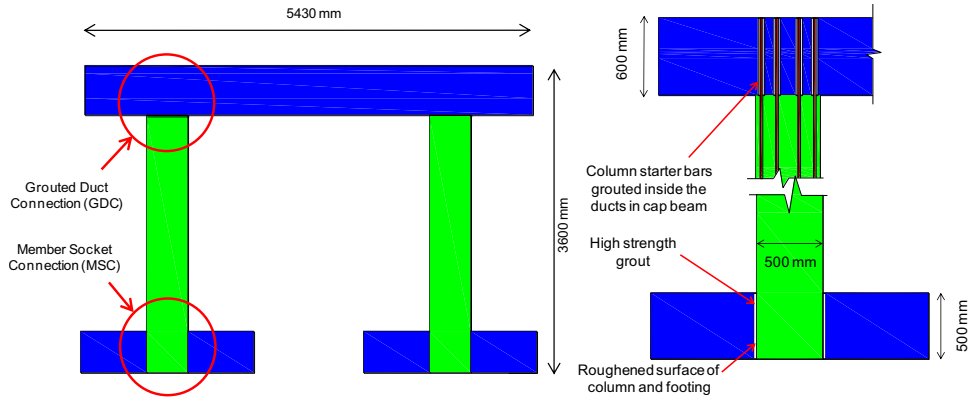

Fig. 5. Dimensions of half-scale specimen.

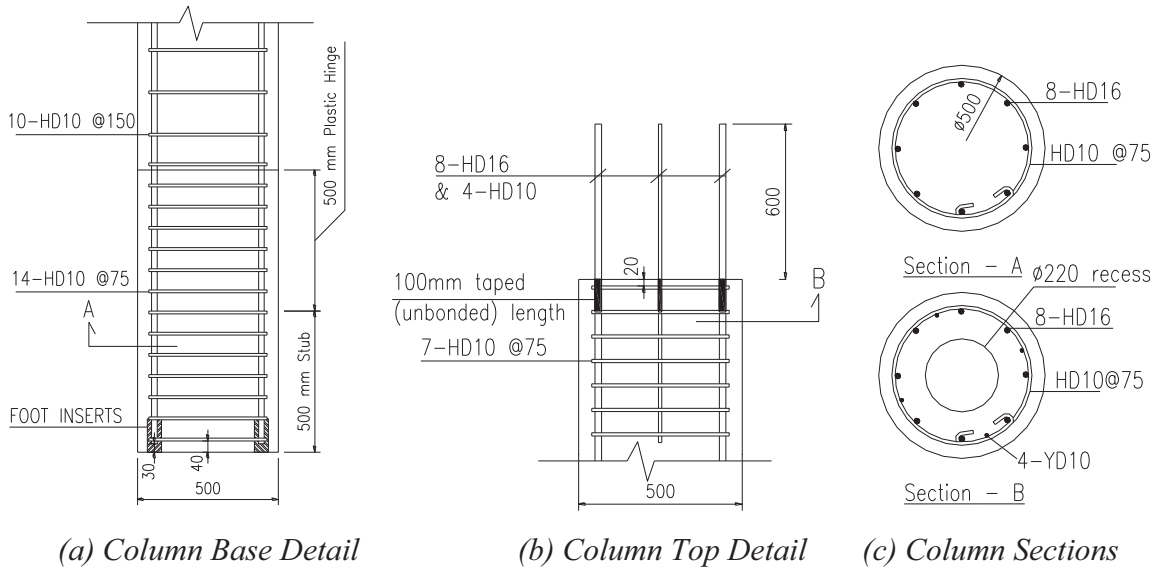

Fig. 6. Precast column details.

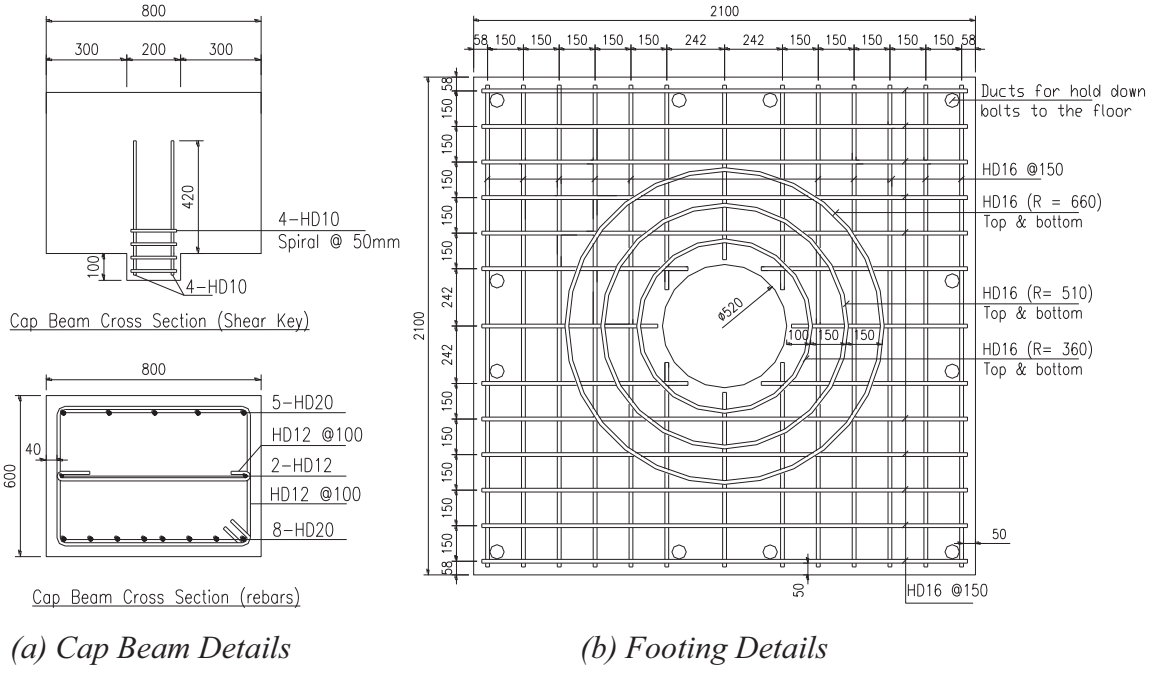

Fig. 7. Precast cap beam and footing details.

The overall flexural and shear designs of the column, cap beam, and footing can be done similar to those for reinforced concrete design of cast-in-place elements. For design of the footing with socket, [8] explained that during lateral loads, bearing stresses are induced in the socket. In addition to compressive stresses in the radial direction, there are hoop tensile stresses around the footing socket which are perpendicular to the compressive bearing stresses. As the tensile capacity of concrete is negligible, the hoop stresses can cause radial cracking near and around the footing socket which would eventually extend to the perimeter of the footing. In order to prevent from the radial cracking of the footing, circular hoop bars can be provided on top and bottom layers of the reinforcing bars (Fig. 7b). For a maximum efficiency, the rebars should be orientated tangentially to the hoop stresses.

Figs. 6 and 7 present reinforcing details for all precast elements.

Figs. 8 and 9 present photos from construction and assembly of the bent, respectively.

5. Testing arrangement and instrumentation

Test setup is illustrated in Fig. 10. Lateral loads are represented by a horizontal actuator with 1000 kN capacity. The vertical actuator exerts gravity loads on the specimen. The specimen was tested under quasi-static cyclic loading with increasing drift ratios (Fig. 11c). The loading protocol was adopted from the ACI Innovation Task Group 1 [31].

Instrumentation of the specimen included attachment of a variety of sensors such as load cells, linear potentiometers, and strain gauges on the specimen. The sensors recorded deformations and forces in the specimen during testing. There were two load cells, one per each ram, to record the lateral and gravity loads on the bent during testing (Fig. 10b).

Fig. 8. Photos from construction of precast elements in the bent.

Flexural and shear deformation of the bent was measured using vertical, horizontal, and diagonal array of linear potentiometers (Fig. 10d–g). Each plastic hinge had six potentiometers attached on the south face (Fig. 10f), two on the north side (Fig. 10g), and two on the west side (Fig. 10e).

String potentiometers were provided to record global displacements of the bent in the east-west and north-south directions. Two string potentiometers, one per each column, were attached to independent frames behind the bent to monitor out-of-plane displacements (Fig. 10d–e). Another string potentiometer was installed to an independent frame to record the in-plane displacement of the bent (Fig. 10f–g).

Four spring-loaded potentiometers were mounted in the strong floor to monitor any slide in the footings during testing (Fig. 10d). Many other potentiometers were mounted on the face of the cap beam on the north and south sides to record deformations of the cap beam (Fig. 10f–g).

Strain gauges were installed on the reinforcing bars of the columns at the plastic hinging zones. Strain gauges were intended as a backup source for collecting the data from the columns during testing. In Fig. 10d–g, the horizontal and vertical arrows represent locations of lateral and gravity rams, respectively.

(a) Precast Elements (b) Footings Secured (c) Column Assembly

(d) Roughened Surface of Column (e) Columns Erected (f) Cap Beam Installation

(g) Guiding Column Starter Bars into the Ducts (h) Column-to-Cap Beam Sealed

(i) Grouting of Bottom and Top Connections (j) Completed Precast Bent

Fig. 9. Photos from assembly of the bent.

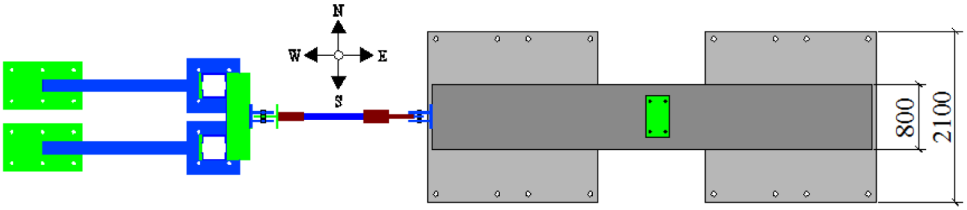

(a) Plan View

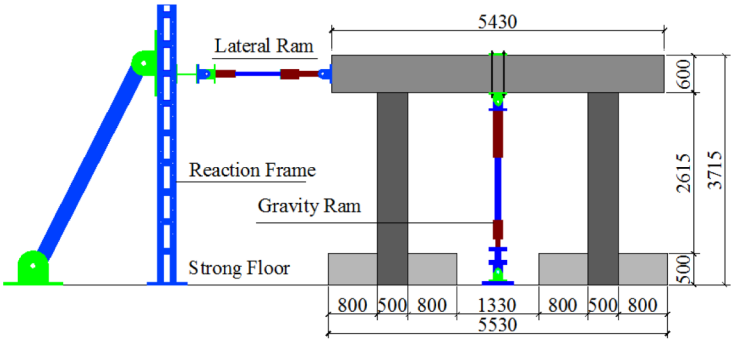

(b) Elevation View

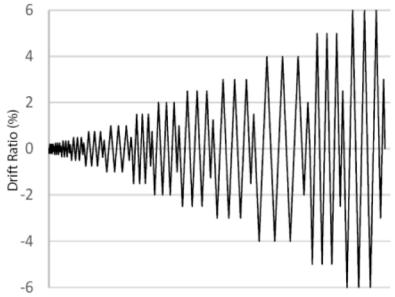

(c) Loading Protocol

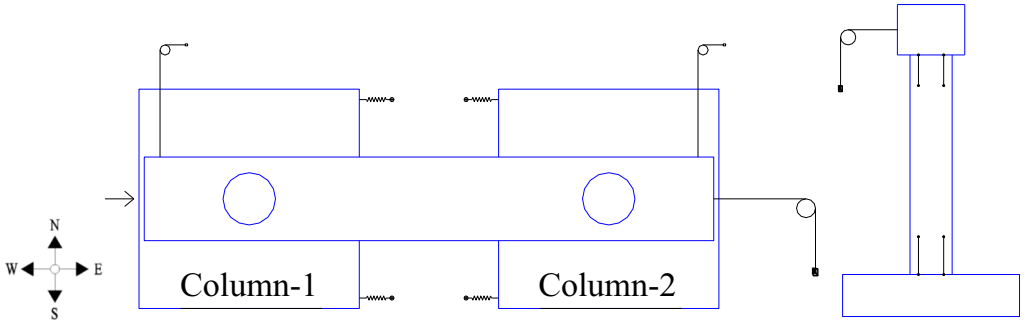

(d) Plan View

(e) West Side

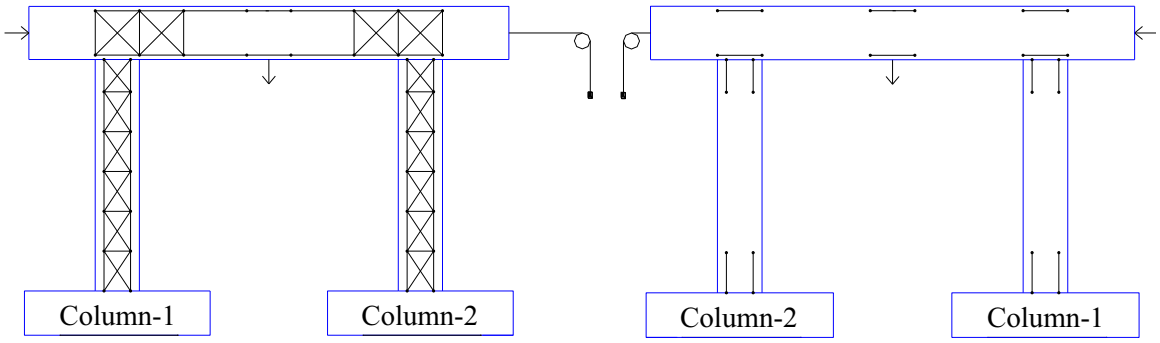

(f) South Side

(g) North Side

Fig. 10. Testing arrangement and instrumentation.

6. Experimental results

For the bottom Member Socket Connections (MSCs), minor flexural cracks appeared during cycles of 0.2% drift ratio. Further cracking occurred with increasing drift ratios. For the top Grouted Duct Connections (GDCs), flexural cracks started at a similar drift ratio (0.2%).

For MSCs, larger cracks were located at the plastic hinge zone. The height of spalling was taken as the plastic hinge length for a visual inspection. Using a measuring tape, the observed plastic hinge length was approximately equal to the diameter of the column section (500 mm). According to NZS 3101 [29], similar plastic hinge length would be expected from a ductile monolithic column incorporating unidirectional plastic hinge.

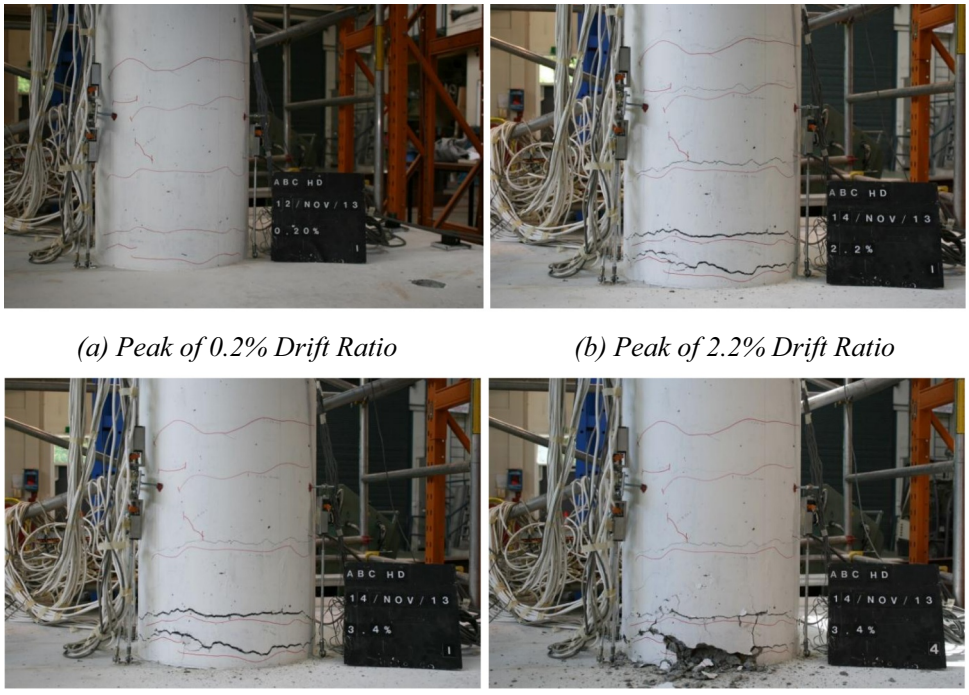

(a) Peak of 0.2% Drift Ratio *(b) Peak of 2.2% Drift Ratio*

(c) Peak of 3.4% Drift Ratio *(d) End of 3.4% Drift Ratio*

Fig. 11. Damage progression in Member Socket Connections (MSCs).

Table 2
Summary of observed damage in plastic hinges.

	Drift ratios (%)							
	0.35	**0.5**	**1.0**	**1.5**	**1.8**	**2.2**	**2.8**	**3.4**
Column-to-Cap Beam GDC Cracks (mm)	< 0.4	0.4	0.5	1.5	4	6	7	Spall
Column-to-Footing MSC Cracks (mm)	< 0.4	0.4	2	3	8	Spall	Spall	Spall

For GDC, there were few large cracks opening and closing with increasing drift ratios. The cracks were concentrated in the region where the starter bars were unbonded. The column plastic hinge length was measured to be approximately half-diameter of the column section (250 mm) from the bottom face of the cap beam.

There were some hairline cracks up height of the columns. The cap beam and footings remained intact. Some hairline diagonal cracks were observed at panel zones in the cap beam. Testing was stopped following cycles of 3.4% drift ratios. Table 2 presents summary of damage observed at the plastic hinges for each connection type. Figs. 11 and 12 show propagation of damage in the plastic hinges during peak drift ratios and at the end of testing for GDC and MSC, respectively. By the end of testing, spalling had occurred in all four plastic hinges. Buckling of rebars was observed in the bottom MSCs (Fig. 13a). Fig. 13c presents extent of damage in the overall bent following testing.

Mashal et al. [8] performed punching shear tests on member socket connections that were subjected to uni and bi-directional lateral loading. The purpose of the test was to demonstrate the residual shear capacity between the column stub and footing. Experimental results showed no slip of the column inside the socket under punching shear (pull through) load condition to a force level much larger than gravity loads from the superstructure.

Force-drift hysteresis and backbone plots for the precast bent, are shown in Fig. 14. The specimen reached its design base shear of 305 kN. The plots suggest that the bent reached the yield point at 0.85% drift ratio. The Ultimate Limit State (ULS) was taken as the drift ratio (2.2%) where spalling initiated in the plastic hinges. The displacement ductility at ULS was therefore 2.6. Maximum Considered Earthquake (MCE) was taken as the drift ratio at the end of testing (3.4%). The displacement ductility at MCE was 4.

As it can be observed from the force-drift hysteresis (Fig. 14a), there were large residual displacements in the bent after the yield point. The residual displacements in the bent were approximately 50% of the peak drift during cycles of 2.8% and 3.4% drift ratios.

It should be noted that in Fig. 14 plots, the positive vertical axis represents the specimen in pulling. For each cycle at each inputted drift ratio, the specimen was pulled first and then pushed. The reason behind the specimen being slightly stronger in pulling than pushing in Fig. 14b, was the softening effects following the pulling stage.

The progression of yield at each plastic hinge can be observed from the moment-curvature plots in Fig. 15. It is reasonable to assume that each column would resist half of the base shear force in the bent. The inflection point has been taken as the mid-height of the column. The letters “A”, “B”, “C”, and “D”, show the sequence of yield progression at the plastic hinges in the bent. Moment-curvature plots were constructed using the data from the external potentiometers for each plastic hinge zone, and utilizing strain compatibility relationship for reinforced concrete sections.

From Fig. 15 plots, it can be noticed that the top GDCs had slightly less strength degradation compared to the bottom MSCs. This is

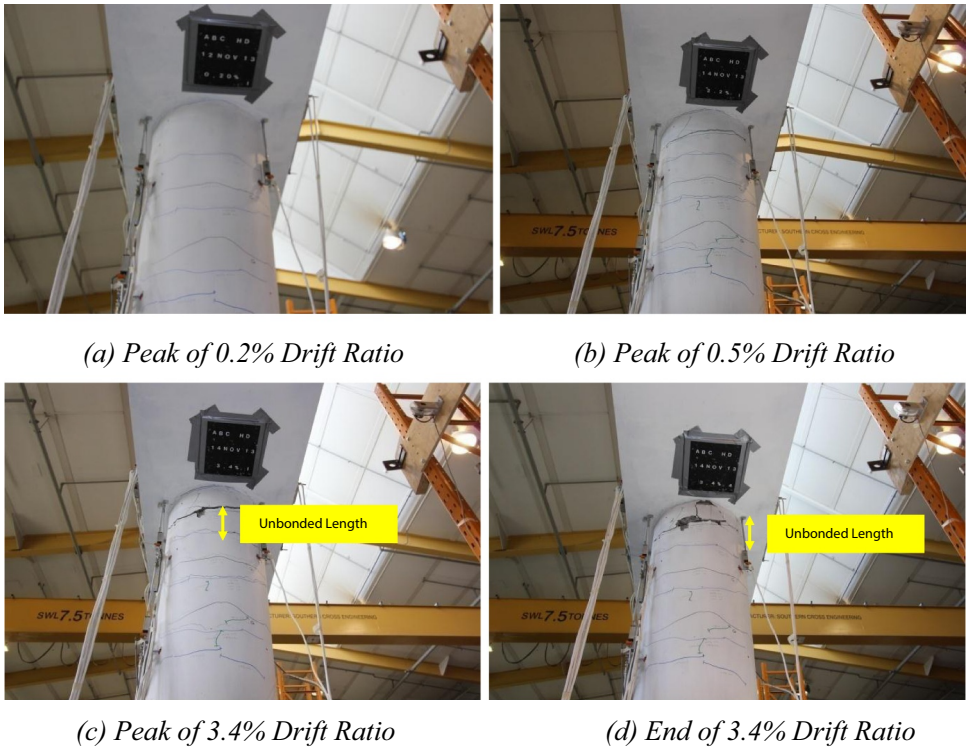

(a) Peak of 0.2% Drift Ratio (b) Peak of 0.5% Drift Ratio

(c) Peak of 3.4% Drift Ratio (d) End of 3.4% Drift Ratio

Fig. 12. Damage progression in Grouted Duct Connections (GDCs).

(a) Bottom MSC (b) Top GDC (c) Locations of Plastic Hinges in the Bent

Fig. 13. Extent of damage to the specimen following testing.

compatible with the extent of damage and spalling observed for each connection during testing (Figs. 11–13). Less strength degradation in GDCs can be attributed with the unbonded length of the starter bars. This effect was noticed by Mashal et al. [8] in testing of cantilever columns with GDCs subjected to similar loading protocol.

In Fig. 15c, it is also obvious that Column-1 MSC had gone through more deformation (highest curvature value and strength degradation) compared to the other three connections. The higher curvature values for this connection can be related to factors such as variation in construction and proximity of the connection to the loading point (lateral actuator).

From Fig. 15 plots, it can be noticed that overall both types of connections (GDC and MSC) had similar moment-curvature response. As presented in Table 2, GDC had fewer cracks compared to MSC. However, the unbonded length of the starter bars in GDCs played a role in having curvature values similar to that in MSC. At the same time, the bent was symmetrical, and both types of connections had similar moment capacities due to almost identical number of flexural reinforcing, refer to Fig. 7.

The corrected area-based damping (hysteretic damping) for the bent was calculated in accordance with Priestley et al. [32]. The bent achieved a hysteretic damping of 13.5% at a displacement ductility of 4.3 which corresponded to 3.4% drift ratio (1.5 times ULS). Fig. 16 presents damping plots for the bent. For a comparison, theoretical damping curves for Takeda-Fat (e.g. reinforced concrete beam) and Takeda-Thin (e.g. reinforced concrete column), are also constructed using the Dwairi-Kowalsky damping rule [33]. The experimental hysteretic damping curve for the bent was higher than that of Takeda-Thin up to a ductility of 1.6. The experimental curve was located just under Takeda-Thin up to a ductility of 4.2. Following that, the curve located between the Takeda-Thin and Takeda-Fat curves. It should be noted that the theoretical hysteretic damping curves in Fig. 16 are plotted for an assumed effective period (T_{eff}) of 1.0 s or larger for the structure. The Equivalent Viscous Damping (EVD) at each drift ratio was calculated in accordance with Priestley et al. [32] as well. EVD is plotted in Fig. 16b.

The energy dissipated per each cycle of each drift ratio for the bent

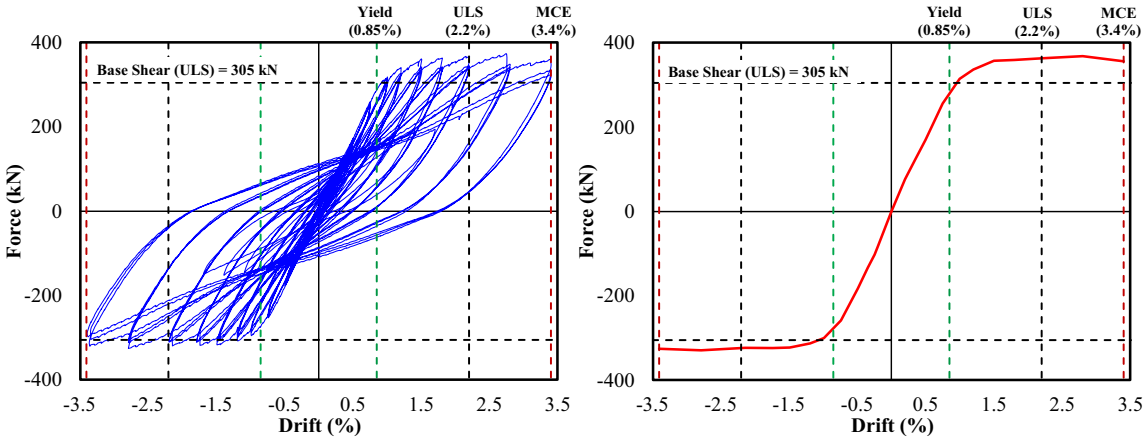

(a) Force-Drift Hysteresis *(b) Backbone-Curve*

Fig. 14. Force-drift hysteresis and backbone-curve.

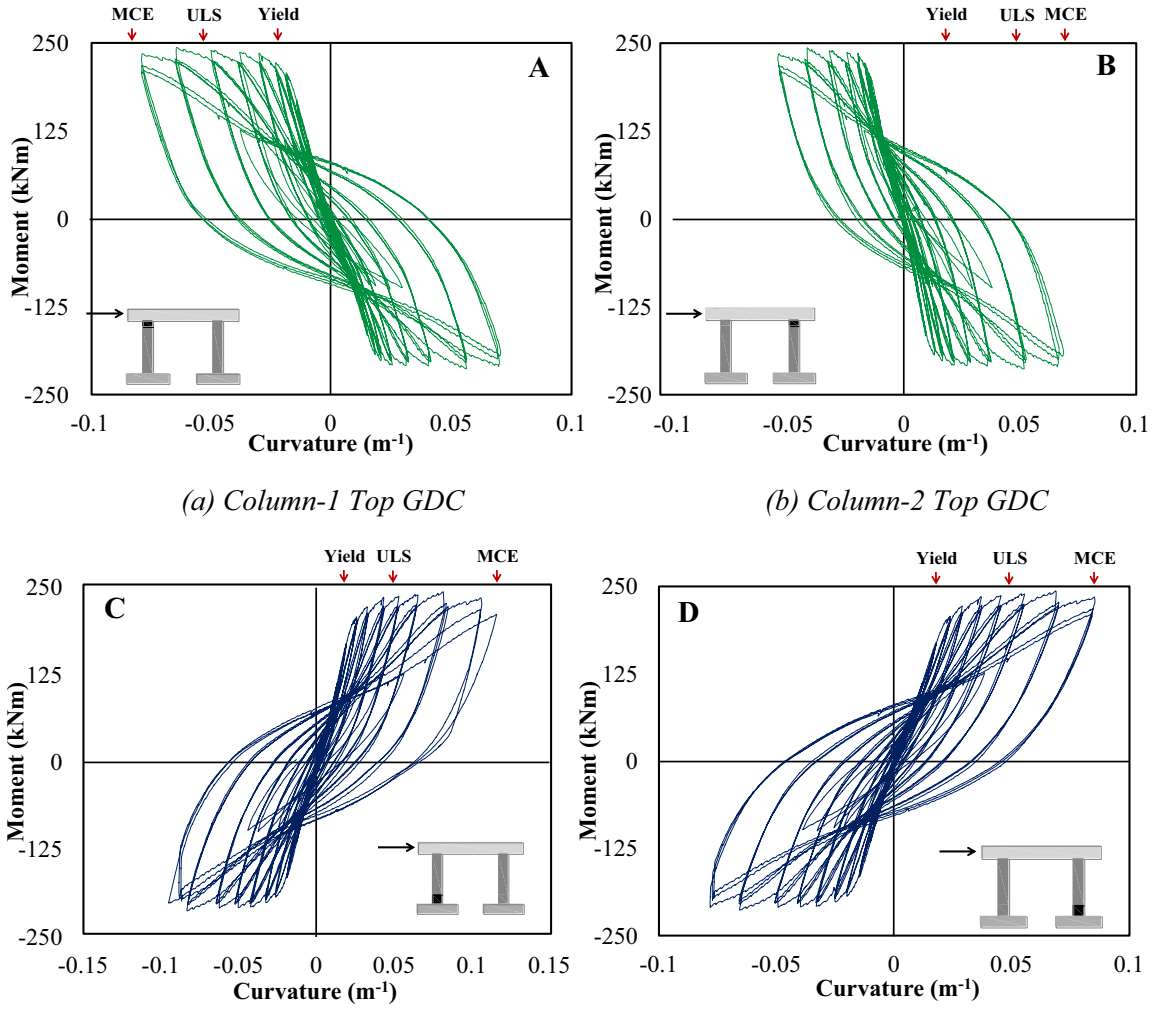

(a) Column-1 Top GDC *(b) Column-2 Top GDC*

(c) Column-1 Bottom MSC *(d) Column-2 Bottom MSC*

Fig. 15. Moment-curvature hysteresis.

is presented in Fig. 17. The dissipated energy was calculated using a numerical integration of the area enclosed inside the hysteresis loop for each four cycles at each drift ratio. It should be noted that the fourth cycle at each drift ratio had half of the amplitude of that drift ratio as explained in the previous section.

7. Progressive collapse analysis

A progressive collapse analysis of the bent was carried out using the procedure outlined in Austroads Technical Report [34]. The methodology incorporates a displacement-based approach and presents strain

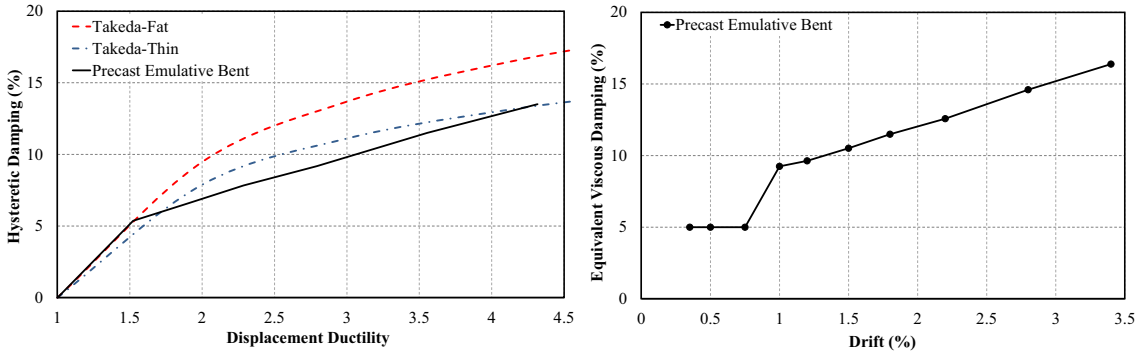

(a) Corrected Area-Based Hysteretic Damping, ξ_{hyst} *(b) Equivalent Viscous Damping, ξ_{eq}*

Fig. 16. Damping curves.

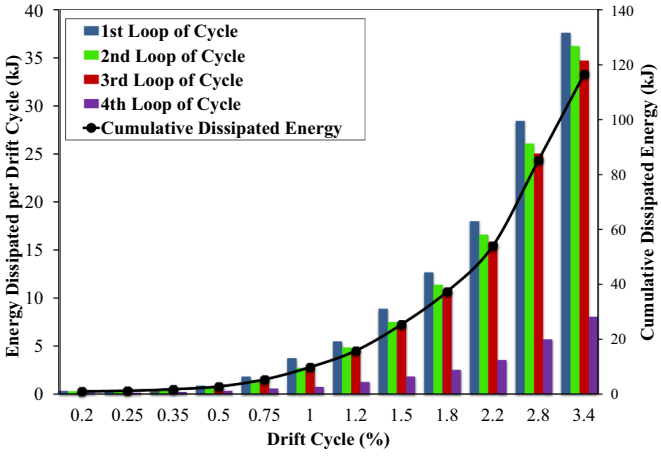

Fig. 17. Energy dissipation plot.

limits for the reinforcing bars and concrete at the Serviceability and Ultimate Limit States. Using the displacement-based procedure of Austroads Technical Report [34], a summary of material strain limits with the qualitative performance description (crack widths) for each performance level are presented in Table 3.

In Accordance with Austroads Technical Report [34], the yield displacement was calculated to be 24 mm (0.82% drift ratio) for the bent. This is very close to the value (0.85%) from experimental force-drift hysteresis (Fig. 14a).

Table 4 presents a summary of the progressive collapse analysis for the bent in accordance with Austroads Technical Report [34]. Since the bent was tested up to 3.4% drift ratio, the MCE level was taken as this drift ratio which corresponded to 1.25 times ULS drift ratio.

Fig. 18 presents the deformed shape and progression of force-displacement hysteresis from experimental testing at each performance limit states. The location of plastic hinges in the bent is shown by circles.

8. Acceleration-Displacement Response Spectrum Analysis (ADRS)

ADRS was carried out in accordance with Marriott [35] to provide further information to assess the performance of the bent under various seismic hazards from NZS 1170.5. Fig. 19 presents plots for ADRS. A summary of findings are provided in Table 5. It can be noticed that results from ADRS plots in Fig. 19 are well correlated with the findings from the progressive collapse analysis of the bent as presented in Table 4 previously.

Table 3
Summary of strain limits and associated crack widths for performance levels.

Limit states	Reinforcing steel strain (ε_s)	Concrete strain (ε_c)	Crack width (mm)	Operational performance level	Repair strategy
Yielding	0.00275	< 0.004	< 1	Fully Operational	No repair/limited epoxy injection
Serviceability	0.015	0.004	1–2	Delayed Operational	Epoxy injection/concrete patching
Ultimate Limit State	0.0448	0.0176	> 2	Delayed Operational	Extensive repair/reconstruction
Maximum Considered Earthquake	> 0.05	–	Spall	Delayed Operational	Extensive repair/reconstruction

Table 4
Summary of Progressive Collapse Analysis.

Limit States	**Yield**		**Serviceability**		**Ultimate limit state**		**Maximum considered earthquake**	
Status	**Fully operational**		**Delayed operational**		**Delayed operational**		**Delayed operational**	
Drift (%)	0.82		1.5		2.7		3.4	
Ductility (μ)	1.0		1.8		3.3		4.1	
Moment Capacity	180 kNm		232 kNm		240 kNm		225 kNm	
Strain limits (ε)	ε_c	ε_s	ε_c	ε_s	ε_c	ε_s	ε_c	ε_s
	< 0.004	0.00275	0.004	0.015	0.0176	0.0448	–	> 0.05
Location	GDC	MSC	GDC	MSC	GDC	MSC	GDC	MSC
Crack (mm)	0.5	1.5	1.5	3	7	Spall	9	Spall

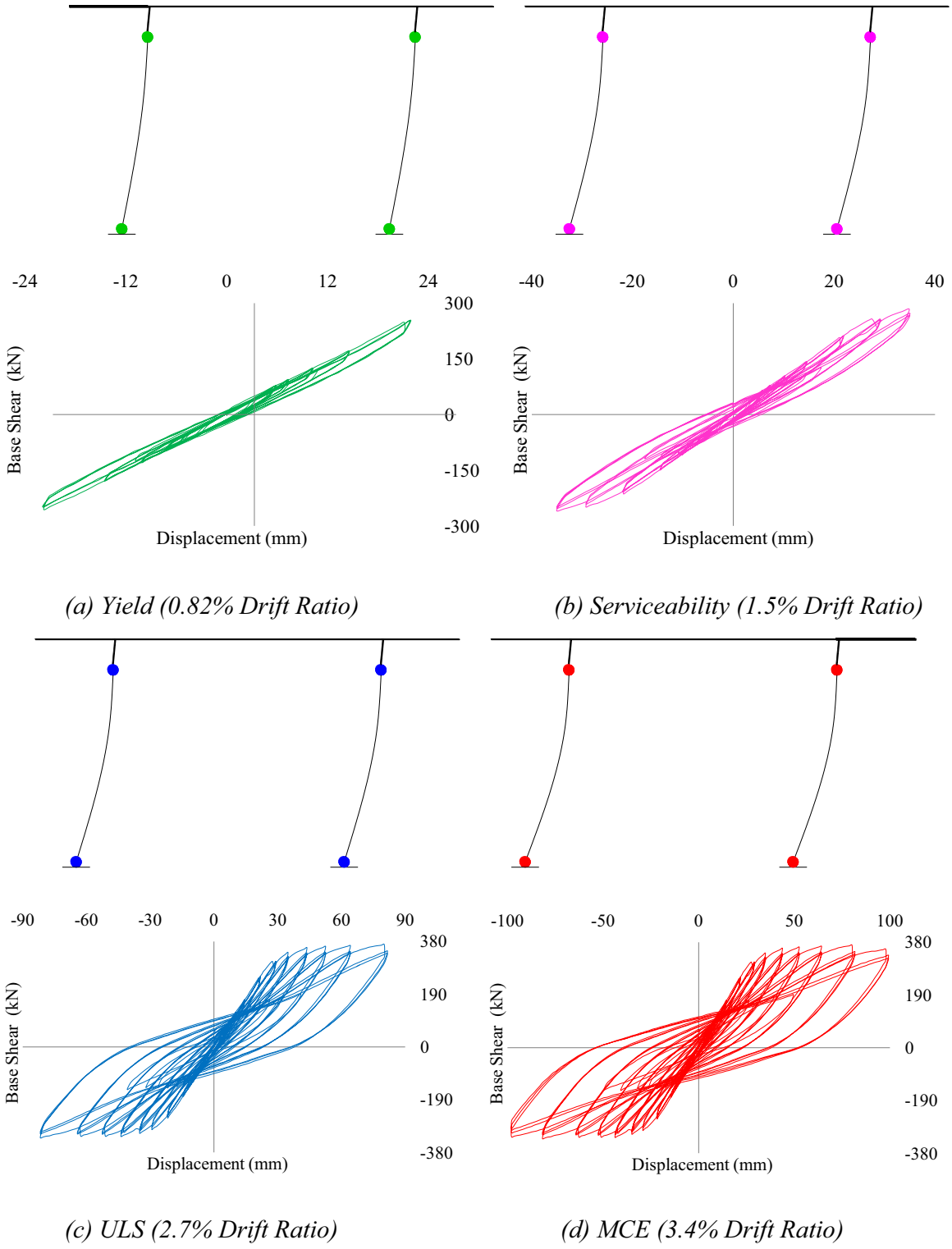

Fig. 18. Deformed shape and force-drift hysteresis at various limit states.

9. Implementation of emulative cast-in-place connections

Grouted ducts and member socket connections have been used in construction of an actual bridge on Interstate Highway 5 in the State of Washington in the United States (Fig. 20). The bridge is located in a seismic region. The arrangement of the connections in this bridge is similar to the specimen tested in this research. The bridge incorporated member socket connection for the column-to-footing; and grouted ducts connection for the column-to-cap beam. The footing was poured around the precast column in this bridge. Also, the cap beam was partially precast. The upper portion of the cap beam was poured on-site which connects the superstructure girders.

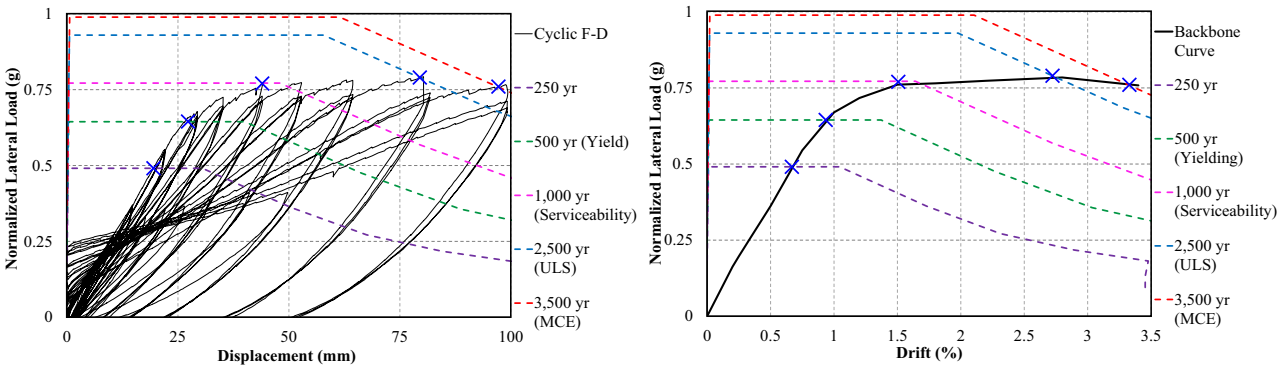

(a) Normalized Force-Displacement Hysteresis (b) Normalized Force-Drift Backbone Curve

Fig. 19. ADRS plots.

Table 5
Summary of ADRS results.

Hazard levels (Years)	Return period factor (R)	Ductility (μ)	Drift (%)	Corrected equivalent damping (ξ_{eq}) %
250	0.75	1	0.67	10.37
500	1.0	1.18	0.93	10.75
1000	1.3	1.9	1.5	13
2500	1.8	3.5	2.7	17.85
3500	2.0	4.2	3.33	19.67

Fig. 20. Precast bent with member socket and grouted duct connections on I-5 in the State of Washington, after Haraldsson et al. [20].

10. Summary of research contributions

The research in this paper aims to contribute in wider adoption of emulative cast-in-place connections for ABC. Experimental testing was carried out to validate seismic performance of grouted ducts and member socket connections in a precast bent. The research presented design considerations and detailing such as leaving unbonded length in the starter bars and roughening of the socket walls, for a better seismic performance of the structure. Furthermore, detailed construction sequence was presented to highlight the emulative cast-in-place technology. Displacement-based seismic assessment was used to compare capacity versus demand for a variety of earthquake return periods. Progressive collapse analysis was done to illustrate performance-based seismic design approach for a precast bent incorporating emulative

cast-in-place connections.

11. Conclusions

Accelerated Bridge Construction (ABC) offers many advantages such as rapid construction, minimum traffic disruptions, improved quality, and durability. ABC has been deployed in low seismic regions. However, given the uncertainty on performance of the connections between precast elements, application of ABC in seismic regions has been limited. The research experimentally tested a concept proposed for a precast bent in seismic regions. A half-scale precast bent was tested under gravity and lateral loads. The column-to-footing connection was member socket, while the column-to-cap beam connection was grouted ducts. Experimental results showed good performance of the specimen. The bent exhibited a stable hysteresis with good levels of ductility and energy dissipation by formation of plastic hinges in the columns. This was similar to what can be expected from a cast-in-place (monolithic) construction. There was no inelastic deformation concentrated in the elements which were designed to be capacity protected (e.g. footings and cap beam). Comparing experimental results to a theoretical model (Takeda-Thin) for cast-in-place construction, the bent had slightly lower energy dissipation only to a certain level of ductility (e.g. 4.25). Following that, the bent had higher energy dissipation. There were multiple large cracks at the plastic hinge zones where member socket connections were used. For grouted duct connections, there were only a few large cracks opening and closing during the testing. Member socket connections had higher strength degradation and spalling compared to grouted duct connections. The reason for this was due to debonding of the starter bars at the column-to-cap beam connections. The study showed once again that leaving an unbonded length of the starter bars in a grouted ducts connection can result in less strength degradation and spalling in the column plastic hinge. The research used an unbonded length of 100 mm in the starter bars. More research work is required to quantify appropriate strain limits and unbonded length for a variety of rebar diameters. For member socket connection, roughened surface with exposed aggregates around the column stub and foundation socket walls, would provide better bond for the connection. The exposed aggregates surfaces should be left in saturated surface dry condition before pouring grout. The socket depth would have to be sufficient enough to prevent from punching shear (pull through) failure of the column under gravity loads. The research maintained a ratio of 1:1 between the socket depth and column diameter. Additional research work is required to investigate the performance of the connection under a variety of socket depth to column diameter ratios. The gap between the column stub and socket wall would have to be sufficient enough to pour the grout and agitate it with a thin flat bar. In this research, a 10 mm gap was used. More research is needed to investigate the performance of the sockets with larger gaps. There is no rebars crossing the footing to column interface in a member socket connection. Therefore, in terms of durability it is thought to offer a better performance compared to cast-in-place construction. To provide a better performance under the freeze-thaw cycles, a low shrinkage grout can be used to grout the socket. However, this would require further studies on the durability aspects of the connection. Overall, the bent investigated in this research satisfied the criteria for operational performance levels. This means if used in an actual bent, the bridge would remain open to traffic with delayed or limited functionality after a design level earthquake. The bridge would not collapse during a maximum considered earthquake. This is similar to the current widely practiced philosophy for seismic design of cast-in-place bridges. Observations from testing and experimental results showed that the emulative bent would have residual displacement following a large earthquake. The bridge would need extensive repair or possible replacement, similar to what can be expected of cast-in-place construction. However, the emulative bent offers the advantage for precasting.

Acknowledgments

The authors would like to acknowledge support from the University of Canterbury, New Zealand's Ministry of Science and Innovation – Natural Hazards Research Platform (NHRP), and technicians Gavin Keats and Russell McConchie for helping with the testing.

Funding

This work was supported by the New Zealand's Ministry of Science and Innovation – Natural Hazards Research Platform (NHRP); and the University of Canterbury Doctoral Scholarship.

References

[1] Billington SL, Barnes RW, Breen JE. A precast segmental substructure system for standard bridges. PCI J 1999;44:56–73. https://doi.org/10.15554/pcij.07011999.56.73.
[2] Billington SL, Barnes RW, Breen JE. Alternate substructure systems for standard highway bridges. J Bridg Eng 2001;6:87–94. https://doi.org/10.1061/(ASCE)1084-0702(2001)6:2(87).
[3] Wacker JM, Hieber DG, Stanton JF, Eberhard MO. Design of precast concrete piers for rapid bridge construction in seismic regions. Res Rep 2005.
[4] Restrepo JI, Tobolski MJ, Matsumoto EE. NCHRP Report 681: Development of a precast bent cap system for seismic regions.pdf. <https://doi.org/10.17226/14484>; 2011.
[5] Marsh ML, Stanton JF, Wernli M, Eberhard MO, Garrett BE, Weinert MD. Application of accelerated bridge construction connections in moderate-to-high seismic regions. Washington, DC: The National Academies Press; 2011. https://doi.org/10.17226/14571.
[6] Palermo A, Mashal M. Accelerated bridge construction (abc) and seismic damage resistant technology: a New Zealand challenge. Bull New Zeal Soc Earthq Eng 2012;45:123–34.
[7] Sideris P, Aref AJ, Filiatrault A. Large-scale seismic testing of a hybrid sliding-rocking posttensioned segmental bridge system. J Struct Eng 2014;140:04014025. https://doi.org/10.1061/(ASCE)ST.1943-541X.0000961.
[8] Mashal M, White S, Palermo A. Quasi-static cyclic testing of cast-in-place emulative connections for accelerated bridge construction in seismic regions. Bull New Zeal Soc Earthq Eng 2016;49(3).
[9] Haber ZB. Precast column-footing connections for accelerated bridge construction in seismic zones. ProQuest Diss Theses 2013:661.
[10] Khaleghi B. Highways for life projects and accelerated bridge construction in Washington state. Trb 2011;7181:1–12.
[11] Buckle I. The Northridge, California earthquake on january 17: Performance of highway bridges; 1994.
[12] Wood SL, Stanton JF, Hawkins NM. Performance of precast parking garages in the Northridge earthquake: lessons learned. In: Proceedings14th Struct. Congr. Part 1 (of 2), vol. 2; 1996, p. 1221–7.
[13] Matsumoto EE, Waggoner MC, Sumen MEK G,Wood SL, JEB. Development of a Precast Bent Cap System. vol. 7; 2001.
[14] Matsumoto E, Kreger M, Waggoner M, Sumen G. Grouted connection tests in development of precast bent cap system. Transp Res Rec 2002;1814:55–64. https://doi.org/10.3141/1814-07.
[15] Brenes FJ, Wood SL, Kreger ME. Anchorage Requirements for Grouted Vertical-Duct Connectors in Precast Bent Cap Systems: A Summary; 2006.
[16] Riva P. Seismic behaviour of precast column-to-foundation grouted sleeve connections. Solid Mech Appl 2006;140:121–8. https://doi.org/10.1007/1-4020-4891-2_10.
[17] Culmo P. M. Connection Details for Prefabricated Bridge Elements and Systems; 2009.
[18] Steuck KP, Stanton JF. Rapidly Constructible Large-Bar Precast Bridge-Bent Seismic Connection; 2008.
[19] Pang JBK, Eberhard MO, Stanton JF. Large-Bar Connection for Precast Bridge Bents in Seismic Regions; 2010. p. 231–9. doi:<http://doi.org/10.1061/(ASCE)BE.1943-5592.0000081>.
[20] Haraldsson OS, Janes TM, Eberhard MO, Stanton JF. Seismic resistance of socket connection between footing and precast column. Am Soc Civ Eng 2013;18:910–9. https://doi.org/10.1061/(ASCE)BE.1943-5592.0000413.
[21] Marson J, Bruneau M. Cyclic testing of concrete-filled circular steel bridge piers having encased fixed-based detail. J Bridg Eng 2003:14–23. https://doi.org/10.1061/(ASCE)1084-0702(2004)9:1(14).
[22] Kingsley AM. Experimental and Analytical Investigation of Embedded Column Base Connections for Concrete Filled High Strength Steel Tubes; 2005.
[23] Zhu Z, Ahmad I, Mirmiran A. Seismic performance of concrete-filled FRP tube columns for bridge substructure. J Bridg Eng 2006;11:359–70. https://doi.org/10.1061/(ASCE)1084-0702(2006)11:3(359).
[24] Nelson M, Lai YC, Fam A. Moment connection of concrete-filled fiber reinforced polymer tubes by direct embedment into footings. Adv Struct Eng 2009;11:537–47. https://doi.org/10.1260/136943308786412023.
[25] Roeder CW, Lehman DE, Thody R. Composite action in CFT components and connections. Eng J 2009;46:229–42.

[26] NZTA. Standard Precast Concrete Bridge Beams. Wellington; 2008.
[27] NZTA. New Zealand Bridge Manual, 3rd Edition; 2014.
[28] Standards NZ. Structural design actions-earthquake actions. Wellington: New Zealand Standards; 2004.
[29] Standards NZ. The design of concrete structures. Wellington: Standards New Zealand; 2006.
[30] Mashal M, White S, Palermo A. Accelerated bridge construction and seismic low-damage technologies for short-medium span bridges. In: Proceedings of the 37th IABSE Symp Eng Progress, Nat People; 2014. p. 1208–15. doi:<http://doi.org/10.2749/222137814814067707>.
[31] ACI T1.1-01. Acceptance Criteria for Moment Frames Based on Structural Testing; 2001.
[32] Priestley MJN, Calvi GM, Kowalsky MJ. Displacement-based seismic design of structures; 2007.
[33] Dwairi HM, Kowalsky MJ, Nau JM. Equivalent damping in support of direct displacement-based design. J Earthq Eng 2007;11:512–30. https://doi.org/10.1080/13632460601033884.
[34] Austroads. Bridge design guidelines for earthquakes. Sydney: Austroads; 2012.
[35] Marriott. The Development of High-Performance Post-Tensioned Rocking Systems for the Seismic Design of Structures; 2009.